Manipulating torsional motions of soft dielectric tubes

Gal Shmuel

Citation: Journal of Applied Physics **117**, 174902 (2015); doi: 10.1063/1.4919668
View online: http://dx.doi.org/10.1063/1.4919668
View Table of Contents: http://scitation.aip.org/content/aip/journal/jap/117/17?ver=pdfcov
Published by the AIP Publishing

Manipulating torsional motions of soft dielectric tubes

Gal Shmuel[a)]
Faculty of Mechanical Engineering, Technion - Israel Institute of Technology, 32000 Haifa, Israel

(Received 24 February 2015; accepted 22 April 2015; published online 4 May 2015)

Tubular dielectric elastomers function as actuators by application of a radial voltage difference. This work demonstrates how the applied electric field can be exploited to manipulate their torsional motion. The approach employed considers torsional elastic waves superposed on a finitely deformed configuration, which depends on bias electromechanical loadings. The theory of nonlinear electroelasticity is utilized to derive the corresponding governing equations. These are analyzed analytically and numerically, as functions of the thickness of the tube, the mechanical constraints, and most importantly the applied voltage. The analysis shows how dispersive waves beyond a certain length are filtered across a frequency band, and are significantly accelerated above it. This phenomenon observed to strongly depend on the applied voltage, in a non-linear manner. [http://dx.doi.org/10.1063/1.4919668]

I. INTRODUCTION

Dielectric elastomers[1–3] are capable of undergoing large deformations[4] and their electromechanical properties are changed when subjected to electric stimuli. They consist of a soft elastomer coated with flexible electrodes. When a voltage is applied to the electrodes, the dipoles of the deformable dielectric reorient. The resultant polarization tends to weaken the external electric field. To maintain the same voltage difference, additional charge accumulates on the electrodes, leading to enhanced Coulomb forces between the free charges. Consequently, the surfaces of the electrodes are drawn closer, squeezing the elastomer in one direction, expanding it in the transverse ones.[5] Owing to this simple working principle, their low cost, light weight, fast response, and particularly their ability to sustain large strains,[6,7] various mechanisms using soft dielectrics were developed; haptic feedbacks, mini-robots, pumps, and miniature grippers are only a few examples.[8,9]

Tunable dynamic behavior of dielectric elastomers has been extensively investigated recently.[10–14] Heterogeneity has a significant role in this regard, as its modification, in turn, influences the manner waves disperse. It was recently shown, for example, how electrostatic tuning of periodic heterogeneity modifies the frequency range of propagating waves.[15–17] This work exploits electrostatically induced heterogeneity in hollow dielectric elastomer cylinders[5,18,19] to manipulate torsional motions, thus complementing a previous work on longitudinal ones.[20] First, the tube is quasi-statically deformed by means of a radial electric field, where two different mechanical conditions are considered. Subsequently, torsional waves propagating on top of the resultant configuration are analyzed. The significance of the mechanical constraints in the response of soft dielectrics, well-known for the static regime,[21–24] is explored in this setting. Related problems were treated in purely elastic annular cylinders.[25,26] However, the sequel will demonstrate how mechanical waves propagate in a unique manner in electroelastic hollow cylinders. More importantly, it will show how these can be significantly manipulated by tuning the bias electric field. This, in turn, promotes their use for applications such as active isolators, motors, and robot-arms, to name just a few.

The following sections compose the paper. Section II summarizes the required theoretical background in nonlinear electroelasticity and superposed incremental fields.[27–32] Section III revisits a previously reported solution[20] for the static deformation of an electroelastic tube when subjected to a radial electric field, at different mechanical constraints. Section IV begins with the derivation of the equations governing torsional waves superposed on the resultant deformed tube. Subsequently, analytical observations are pointed out for several limiting cases, and a numerical scheme for a solution to the general problem is detailed. Utilizing this scheme, Sec. V numerically investigates the dependency of the characteristics of the motion on the geometry of the tube, the mechanical constraints, and most importantly the bias electric field. Finally, the primary results and conclusions are summarized in Sec. VI.

II. FINITE AND INCREMENTAL ELECTROELASTICITY

Let Ω_0 denote a stress-free reference configuration of an electroelastic body, with a boundary $\partial\Omega_0$. The body deforms to a configuration Ω due to electromechanical loadings. The resultant position of a body particle $\mathbf{x} \in \Omega$ is the image of a twice differentiable vector field $\boldsymbol{\chi}$, acting on a material point $\mathbf{X} \in \Omega_0$, that is, $\mathbf{x} = \boldsymbol{\chi}(\mathbf{X}, t)$. The deformation gradient $\mathbf{F} = \nabla_{\mathbf{X}}\boldsymbol{\chi}$ is used to map geometrical quantities in the vicinity $\mathbf{X}$, where $\nabla_{\mathbf{X}}$ is the gradient operator in the reference configuration. Specifically, infinitesimal line $\mathrm{d}\mathbf{X}$, area $\mathbf{N}\mathrm{d}A$ and volume $\mathrm{d}V$ elements are mapped to their current counterparts $\mathrm{d}\mathbf{x}$, $\mathbf{n}\mathrm{d}a$, and $\mathrm{d}v$ according to $\mathbf{F}\mathrm{d}\mathbf{X}$, $\mathbf{n}\mathrm{d}a = J\mathbf{F}^{-\mathrm{T}}\mathbf{N}\mathrm{d}A$ and $\mathrm{d}v = J\mathrm{d}V$, respectively. Herein, $J \equiv \det\mathbf{F}$, and $\mathbf{N}$ and $\mathbf{n}$ are unit vectors normal to $\mathrm{d}A$ and $\mathrm{d}a$, respectively. In the sequel, the right $\mathbf{C} = \mathbf{F}^{\mathrm{T}}\mathbf{F}$ and left $\mathbf{b} = \mathbf{F}\mathbf{F}^{\mathrm{T}}$ Cauchy-Green strain tensors will be also used.

a)Electronic mail: meshmuel@tx.technion.ac.il

The balance of linear momentum is neatly written in terms of a *total* stress[31] $\boldsymbol{\sigma}$ as

$$\nabla \cdot \boldsymbol{\sigma} = \rho \boldsymbol{\chi}_{,tt}, \tag{1}$$

where mechanical body forces are neglected and ρ denotes the mass density. The total stress, accounting for both mechanical and electrical forces, is symmetric, in virtue of angular momentum balance.

In the body, a prescribed constitutive relation connects the electric vector field, $\mathbf{e}$, and electric displacement field, $\mathbf{d}$. In free space, the vacuum permittivity ϵ_0 is sufficient, such that $\mathbf{d}^\star = \epsilon_0 \mathbf{e}^\star$. Here and in what follows, a star superscript denotes quantities in the surrounding space. For ideal dielectrics, i.e., when there is no free body charge, the quasi-electrostatic approximation of Maxwell equations is

$$\nabla \cdot \mathbf{d} = 0, \quad \nabla \times \mathbf{e} = \mathbf{0}. \tag{2}$$

This approximation is valid when for the same frequency, the length of the mechanical waves is shorter than the electromagnetic waves.

Across the boundary $\partial\Omega$, the foregoing fields are to satisfy the jump conditions

$$[\![\sigma]\!]\mathbf{n} = \mathbf{t}_m, \quad [\![\mathbf{d}]\!] \cdot \mathbf{n} = -w_e, \quad [\![\mathbf{e}]\!] \times \mathbf{n} = \mathbf{0}, \tag{3}$$

where $[\![\bullet]\!] = (\bullet) - (\bullet)^\star$, w_e is the surface charge density, and $\mathbf{t}_m$ is a prescribed mechanical traction. The latter, together with the action of the Maxwell stress $\boldsymbol{\sigma}^\star$ on $\mathbf{n}$, constitutes the total traction on a deformed area element, where

$$\boldsymbol{\sigma}^\star = \epsilon_0 \mathbf{e}^\star \otimes \mathbf{e}^\star - \frac{\epsilon_0}{2}(\mathbf{e}^\star \cdot \mathbf{e}^\star)\mathbf{I}. \tag{4}$$

The *total* first Piola-Kirchhoff stress, the Lagrangian electric displacement, and electric fields

$$\mathbf{P} = J\boldsymbol{\sigma}\mathbf{F}^{-\mathrm{T}}, \mathbf{D} = J\mathbf{F}^{-1}\mathbf{d}, \mathbf{E} = \mathbf{F}^{\mathrm{T}}\mathbf{e}, \tag{5}$$

respectively, satisfy the Lagrangian counterparts of Eqs. (1)–(3)

$$\nabla_{\mathbf{X}} \cdot \mathbf{P} = \rho_L \boldsymbol{\chi}_{,tt}, \quad \nabla_{\mathbf{X}} \cdot \mathbf{D} = 0, \quad \nabla_{\mathbf{X}} \times \mathbf{E} = \mathbf{0}, \tag{6}$$

$$[\![\mathbf{P}]\!]\mathbf{N} = \mathbf{t}_M, \quad [\![\mathbf{D}]\!] \cdot \mathbf{N} = -w_E, \quad [\![\mathbf{E}]\!] \times \mathbf{N} = \mathbf{0}, \tag{7}$$

where $\rho = \rho_L/J$, $\mathbf{t}_M \mathrm{d}A = \mathbf{t}_m \mathrm{d}a$, and $w_E \mathrm{d}A = w_e \mathrm{d}a$. Outside the body, Eq. (5) is evaluated with $\mathbf{F}^\star = \mathbf{F}|_{\partial\Omega_0}$.

The fields $\mathbf{P}$ and $\mathbf{E}$ are the derivatives of Ψ, an *augmented energy density function*[31] of $\mathbf{F}$ and $\mathbf{D}$, namely,

$$\mathbf{P} = \frac{\partial \Psi}{\partial \mathbf{F}}, \quad \mathbf{E} = \frac{\partial \Psi}{\partial \mathbf{D}}. \tag{8}$$

When the solid is incompressible, the stress can no longer be determined as a function of the deformation alone, due to the constraint $J = 1$. Hence, the first of Eq. (8) is replaced with

$$\mathbf{P} = \frac{\partial \Psi}{\partial \mathbf{F}} - p\mathbf{F}^{-\mathrm{T}}, \tag{9}$$

where the Lagrange multiplier p is calculated using the equations of motion together with the jump conditions.

Based on the theory of Dorfmann and Ogden,[32] $\dot{\boldsymbol{\chi}}(\mathbf{X}, t)$ and $\dot{\mathbf{D}}(\mathbf{X}, t)$ are independent small elastic and electric displacement fields, superposed on a static deformed configuration $\Omega(\boldsymbol{\chi})$. Henceforth, overset dot denotes incremental quantities. The *push-forwards* of $\dot{\mathbf{P}}$, $\dot{\mathbf{D}}$, and $\dot{\mathbf{E}}$ are

$$\boldsymbol{\Sigma} = \frac{1}{J}\dot{\mathbf{P}}\mathbf{F}^T, \quad \check{\mathbf{d}} = \frac{1}{J}\mathbf{F}\dot{\mathbf{D}}, \quad \check{\mathbf{e}} = \mathbf{F}^{-T}\dot{\mathbf{E}}, \tag{10}$$

respectively, and satisfy

$$\nabla \cdot \boldsymbol{\Sigma} = \rho \dot{\mathbf{x}}_{,tt}, \quad \nabla \cdot \check{\mathbf{d}} = 0, \quad \nabla \times \check{\mathbf{e}} = \mathbf{0}, \tag{11}$$

where $\dot{\mathbf{x}}(\mathbf{x}, t) \equiv \dot{\boldsymbol{\chi}}(\mathbf{X}, t)$. Incompressibility implies

$$\nabla \cdot \dot{\mathbf{x}} \equiv \mathrm{tr}\mathbf{h} = 0, \tag{12}$$

where $\mathbf{h} \equiv \nabla\dot{\mathbf{x}}$ is the displacement gradient. Upon linearization of the constitutive relations in the increments, the following equations are obtained:

$$\boldsymbol{\Sigma} = \boldsymbol{\mathcal{C}}\mathbf{h} + p\mathbf{h}^{\mathrm{T}} - \dot{p}\mathbf{I} + \boldsymbol{\mathcal{B}}\check{\mathbf{d}}, \tag{13}$$

$$\check{\mathbf{e}} = \boldsymbol{\mathcal{B}}^{\mathrm{T}}\mathbf{h} + \boldsymbol{\mathcal{A}}\check{\mathbf{d}}, \tag{14}$$

where $(\boldsymbol{\mathcal{B}}^{\mathrm{T}}\mathbf{h})_k = \mathcal{B}_{ijk}h_{ij}$. In components form, the instantaneous tensors $\boldsymbol{\mathcal{A}}$, $\boldsymbol{\mathcal{B}}$, and $\boldsymbol{\mathcal{C}}$ are

$$\begin{aligned} \mathcal{A}_{ij} &= JF^{-1}_{\alpha i}\frac{\partial^2\Psi}{\partial D_\alpha \partial D_\beta}F^{-1}_{\beta j}, \\ \mathcal{B}_{ijk} &= F_{j\alpha}\frac{\partial^2\Psi}{\partial F_{i\alpha}\partial D_\beta}F^{-1}_{\beta k}, \\ \mathcal{C}_{ijkl} &= \frac{1}{J}F_{j\alpha}\frac{\partial^2\Psi}{\partial F_{i\alpha}\partial F_{k\beta}}F_{l\beta}. \end{aligned} \tag{15}$$

III. FINITE DEFORMATIONS OF A SOFT DIELECTRIC TUBE IN A RADIAL ELECTRIC FIELD

The finite deformation of a deformable dielectric tube immersed in a radial electric field was first calculated by Singh and Pipkin,[33] revisited later by Zhu *et al.*,[18] and in the framework of small strains by Carpi and De Rossi.[34] Shmuel and deBotton[20] specialized the result of Singh and Pipkin[33] to a particular constitutive law, while accounting for different boundary conditions. In favor of rendering a self-contained report, this section summarizes the solution provided in Sec. III therein.

Consider an incompressible infinite electroelastic tube, coated with compliant electrodes on its inner and outer surfaces at the radii R_A and R_B, respectively (see Fig. 1). When subjected to voltage, a charge per unit length q_A accumulates on the interior electrode. The corresponding electric displacement field in cylindrical coordinate system is

$$\mathbf{d} = d_r\hat{\mathbf{r}} = \frac{q_A}{2\pi r}\hat{\mathbf{r}}, \tag{16}$$

a particle whose initial coordinate is (R, Θ, Z), moves to (r, θ, z), in accordance with

$$r = \sqrt{AR^2 + B}, \quad \theta = \Theta, \quad z = Z/A, \tag{17}$$

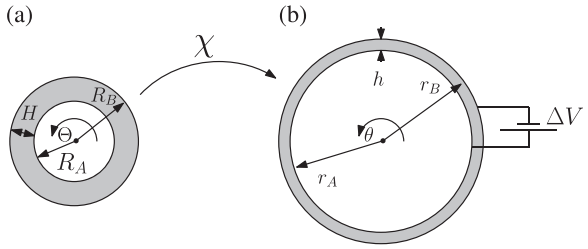

FIG. 1. The polar plane section of the dielectric at (a) the reference configuration, and at (b) the deformed configuration, induced by a voltage ΔV.

where A and B are constants to be determined. The gradient of the deformation (17) in the above coordinate system is diagonal, with the components

$$\lambda_z \equiv F_{zZ} = \frac{1}{A}, \quad \lambda_r \equiv F_{rR} = \frac{AR}{\sqrt{AR^2+B}}, \quad \lambda_\theta \equiv F_{\theta\Theta} = \frac{\sqrt{AR^2+B}}{R}. \tag{18}$$

The constitutive behavior of the tube is assumed to be governed by

$$\Psi_{DH}(\mathbf{F},\mathbf{D}) = \frac{\mu}{2}(\mathrm{tr}\mathbf{C}-3) + \frac{1}{2\epsilon_0\epsilon r}\mathbf{D}\cdot\mathbf{C}\mathbf{D}, \tag{19}$$

where μ and ϵr are the shear modulus and relative dielectric constant, respectively. The associated total stress is

$$\boldsymbol{\sigma} = \mu\mathbf{b} + \frac{1}{\epsilon_0\epsilon r}\mathbf{d}\otimes\mathbf{d} - p\mathbf{I}. \tag{20}$$

When substituted into the equilibrium equations, one finds that

$$p(r) = AB\mu\left(-\frac{1}{2}r^2 + \frac{1}{B}\ln r - \frac{1}{2B}\ln(r^2-B) + \frac{\hat{q}_A}{4}\left(\frac{R_A}{r}\right)^2\right) + P, \tag{21}$$

where $\hat{q}_A = \frac{q_A}{2\pi R_A\sqrt{\mu\epsilon_0\epsilon r}}$. The constants P, A and B are determined using the boundary conditions. There are no prescribed mechanical tractions on the circumferential surfaces, i.e.,

$$\sigma_{rr}|_{r_A} = 0, \quad \sigma_{rr}|_{r_B} = 0, \tag{22}$$

where $r_A \equiv r(R_A)$ and $r_B \equiv r(R_B)$. At this point, two different loading paths are considered, for which the remaining condition differs.

Axially free tube. The tube is free to expand in the axial direction, such that the axial force is zero, namely,

$$\int_0^{2\pi}\int_{r_A}^{r_B}\sigma_{zz} r\,\mathrm{d}r\mathrm{d}\theta = 0. \tag{23}$$

Pre-stretched tube. First, the tube is pre-stretched mechanically in the axial direction, and then clamped at a fixed axial stretch ratio $\tilde{\lambda}_z$. In this manner, $A = 1/\tilde{\lambda}_z$ is a prescribed quantity. Then, the electric load is applied.

The considered constitutive law for the tube admits the following relation between $\mathbf{d}$ and $\mathbf{e}$:

$$\mathbf{d} = \epsilon\mathbf{e}. \tag{24}$$

By its integration, a connection between the voltage and the charge is established, which reads

$$\Delta V = -\int_{r_A}^{r_B} e_r \mathrm{d}r = \hat{q}_A R_A\sqrt{\frac{\mu}{\epsilon_0\epsilon r}}\ln\frac{r_B}{r_A}. \tag{25}$$

In terms of A, B, and the initial geometry, the dimensionless voltage $\Delta\hat{V} \equiv \frac{\Delta V}{H}\sqrt{\frac{\epsilon_0\epsilon r}{\mu}}$ is

$$\Delta\hat{V} = \hat{q}_A\frac{R_A}{H}\ln\frac{\sqrt{AR_B^2+B}}{\sqrt{AR_A^2+B}}, \tag{26}$$

where $H = R_B - R_A$. Beyond a critical amount of voltage, which depends on the geometry of the tube and the axial constraints, the mechanical response of the material cannot balance the pressure induced by the electric field. The tube thus collapses, and the aforementioned mapping no longer provides a solution. The critical loading and its dependency on the aforementioned parameters will turn to have a significant role in the forthcoming dynamic analysis.

For brevity, the components of the instantaneous constitutive tensors are given in the Appendix.

IV. TORSIONAL MOTIONS SUPERPOSED ON A FINITELY DEFORMED DE TUBE

In what follows, the axial propagation of torsional waves on top of the resultant configuration is formulated and determined. Thus, the incremental displacement field has only one component in the tangential direction, i.e., $\dot{\mathbf{x}} = v\hat{\theta}$. Owing to axial symmetry, the governing fields are independent of θ. Hence, the non-zero components of displacement gradient are

$$h_{\theta z} = v_{,z}, \quad h_{\theta r} = v_{,r}, \quad h_{r\theta} = -v/r. \tag{27}$$

The incremental Faraday law motivates a formulation of $\check{\mathbf{e}}$ as (minus) the gradient of a potential $\varphi(r,z,t)$, such that $\check{\mathbf{e}} = -\nabla\varphi$. Utilizing the linearized constitutive law (14), the components of $\check{\mathbf{d}}$ read

$$\check{d}_z = -\epsilon\varphi_{,z}, \quad \check{d}_r = -\epsilon\varphi_{,r}, \quad \check{d}_\theta = -d_r(v_{,r} - v/r). \tag{28}$$

The incremental Gauss equation

$$\check{d}_{z,z} + \check{d}_r/r + \check{d}_{r,r} = 0, \tag{29}$$

is then solved for φ by separation of variables, with the solution

$$\varphi = [N_1 I_0(kr) + N_2 K_0(kr)]e^{-i(\omega t - kz)}, \tag{30}$$

where I_0 and K_0 are the zero order modified Bessel functions of the first and second kind, respectively, and N_1 and N_2 are constants. Herein, the propagation is assumed to be in the positive z-direction, where ω is the angular frequency and k is the wavenumber.

In contrast to the equations for superposed longitudinal waves,[20] the equation for v decouples from those for $\dot{p}$ and

φ, as well as the jump conditions. The remaining equations along r and z relate $\dot{p}$, φ, and their derivatives. These, together with the corresponding jump conditions

$$\begin{aligned} \Sigma_{rr}|_{r=r_A} &= 0, \quad \Sigma_{rr}|_{r=r_B} = 0, \\ \Sigma_{zr}|_{r=r_A} &= 0, \quad \Sigma_{zr}|_{r=r_B} = 0, \end{aligned} \tag{31}$$

show that the incremental pressure and the electric field vanish. The incremental equation of motion along θ

$$\Sigma_{\theta r,r} + \Sigma_{\theta z,z} + \frac{1}{r}(\Sigma_{\theta r} + \Sigma_{r\theta}) = \rho v_{,tt}, \tag{32}$$

governs v, where

$$\Sigma_{\theta r} = \mu\lambda_r^2 v_{,r} - \left(p - \frac{1}{\epsilon}d_r^2\right)v/r, \tag{33}$$

$$\Sigma_{r\theta} = \left(p - \frac{1}{\epsilon}d_r^2\right)v_{,r} - \left(\mu\lambda_\theta^2 - \frac{1}{\epsilon}d_r^2\right)v/r, \tag{34}$$

$$\Sigma_{\theta z} = \mu\lambda_z^2 v_{,z}. \tag{35}$$

I postulate a solution for the displacement field in the form

$$v = g(r)e^{-i(\omega t - kz)}. \tag{36}$$

Upon substitution of Eq. (36) into (32), a linear ordinary differential equation of order two with variable coefficients is obtained for $g(r)$, namely,

$$\begin{aligned} &\left[\lambda_r^2 + 2\left(\hat{q}_A\frac{R_A}{r}\right)^2\right]g'' + \frac{1}{r}\left[A\left(1+\frac{B}{r^2}\right) - 2\left(\hat{q}_A\frac{R_A}{r}\right)^2\right]g' \\ &+ \left[\frac{\omega^2}{c_B^2} - \frac{k^2}{A^2} - \frac{A}{r^2}\left(1+\frac{B}{r^2}\right) + \frac{2}{r^2}\left(\hat{q}_A\frac{R_A}{r}\right)^2\right]g = 0, \end{aligned} \tag{37}$$

where $\lambda_r^2 = A\left(1-\frac{B}{r^2}\right)$, and $c_B = \sqrt{\mu/\rho}$ is the bulk shear wave velocity in an unstretched isotropic elastic dielectric. In this form it is evident how inhomogeneity evolves by application an electric load directly via $\hat{q}_A$, and through the constant B, which increases monotonically with $\hat{q}_A$. Equation (37) together with the jump conditions

$$\Sigma_{\theta r}|_{r=r_A} = 0, \quad \Sigma_{\theta r}|_{r=r_B} = 0, \tag{38}$$

determine the propagation modes and the *dispersion relation*, which relates the frequencies, lengths, and velocities of the waves.

At this point, I make four observations. First, the functional form of Eq. (37) is essentially different from Eq. (3.3) of Shearer *et al.*[26] who analyzed torsional motion superposed on a finitely deformed hyperelastic tube due to pressure differences. This implies that the effect of the electric field is more than inducing hydrostatic loading and modifying material properties; it intrinsically alters the propagation modes, *in a way which cannot be obtained mechanically*.

Second, interestingly, the non-dispersive fundamental mode $g(r) = r$ always satisfies the boundary-value problem, as explained next. Upon substitution of $g(r) = r$ into Eq. (37), the equation is rendered as a sum of the vanishing finite equilibrium equation along r, and $\left(\frac{\omega^2}{c_B^2} - \frac{k^2}{A^2}\right)g$, providing $c = \lambda_z c_B$. The jump conditions are satisfied too, since with $g(r) = r$ these become equal to σ_{rr}, which, in view of the finite static problem, vanishes across the circumferences.

Third, examining Eq. (37) when k approaches infinity, reveals that in the limit of short waves, all higher modes velocities converge to the fundamental one.

Finally, when the cause of the deformation is only mechanical, that is when $A \neq 0$, $\hat{q}_A = 0$ and consequently $B = 0$, the solution of Eq. (37) is

$$\begin{aligned} g(r) = {} & C_1 J_1(A^{2/3}\sqrt{A^2\omega^2/c_B - k^2}\,r) \\ & + C_2 Y_1(A^{2/3}\sqrt{A^2\omega^2/c_B - k^2}\,r), \end{aligned} \tag{39}$$

where J_1 and Y_1 are the first order Bessel function of the first and second kind, respectively, and C_1 and C_2 are integration constants. In the limit of small deformations, i.e., when $A = 1$, Eq. (39), reduces to the classic solution of linear elasticity,[35] as it should.

In general, however, Eq. (37) cannot be solved analytically. To this end, I extend a numerical procedure, originally used for bifurcation problems,[36,37] as follows. First, in terms of the vector

$$\mathbf{y} = \begin{bmatrix} g \\ g' \end{bmatrix}, \tag{40}$$

I represent Eq. (37) as two linear ordinary differential equations of order one, such that

$$y_i'(r) = A_{ij}(r)y_j(r), \quad i = 1,2, \tag{41}$$

with $A_{ij}(r)$ being the coefficient of y_j in the i-th equation. For each value of k, Eq. (41) is then solved numerically for all values of ω, subjected to the initial-like conditions

$$y_i(r_A) = \delta_{im}, \quad i = 1,2, \tag{42}$$

for the two cases $m = 1$ and $m = 2$. A linear combination of the obtained solutions, say, $\sum_{m=1}^{2}\eta_m\mathbf{y}^{(m)}$, is substituted into the jump conditions (38), replacing g and its derivatives. Pairs of $\{k,\omega\}$ for which this substitution yields a vanishing determinant of the coefficients of η_m, i.e., satisfy the jump conditions, constitute the dispersion curves. The scheme was realized using Wolfram Mathematica 10.

V. NUMERICAL INVESTIGATION OF THE DISPERSION CURVES

The influence of the tube geometry and the electromechanical loadings on the superposed motion is explored next. To this end, the dispersion curves are evaluated for different pre-strains and voltages. The role of the wall-thickness is examined by considering two initial thicknesses of $H = 0.1$ mm and 4 mm. For both cases, $R_A = 1$ mm is set. This corresponds to initial ratios of thickness to mean-radius of $\frac{H}{(R_A+R_B)/2} = 0.095$ and 1.33, respectively. In the sequel, these are referred to as the thin and thick tubes, respectively.

The second, third, and fourth modes are displayed, out of an infinite number of subsequent modes, in addition to the fundamental mode. For brevity, higher modes are omitted, as they reproduce similar trends.

Figs. 2(a) and 2(b) display the normalized velocities $\hat{c} = c/c_B$ as functions of the normalized wavenumber $\hat{k} = kH$, for thin and thick tubes free of mechanical traction, respectively. Here and henceforth, the continuous, dotted-dashed (red), and dotted (blue) curves correspond to $\Delta\hat{V} = 0$, $\frac{1}{2}$, and $\frac{2}{3}$, respectively. We observe how the numerical scheme reproduces the analytical result $\hat{c} = \lambda_z$ for the fundamental mode. The axial strain has a stiffening effect on the instantaneous axial modulus. Therefore, the velocities of this mode rise monotonically with the electric potential, as it increases the axial strain. Higher modes undergo steeper rise. This rise depends non-linearly on $\Delta\hat{V}$. Examine, for example, the velocity of the second mode of the thin tube at $\hat{k} = 2$, $\Delta\hat{V} = 2/3$: it is about three times faster than when $\Delta\hat{V} = 0$. Further, it is approximately 1.5 times the counterpart velocity in an elastic tube, whose geometry is identical to the deformed geometry of the electroelastic body. This demonstrates that the enhancement is not only due to the thinning and stiffening of the tube but also by virtue of an inherent change of the governing equation.

Comparison between Figs. 2(a) and 2(b) shows how the increase in the velocity is more pronounced at the thin tube. Intuitively, it agrees with the general understanding that the electrical driving force becomes more significant as the distance between the electrodes is shorter. This is a direct consequence of Coulomb law, stating that the electric force is inversely proportional to the (square of the) distance between charges. Mathematically, it corresponds to Eq. (26), which implies that for a prescribed $\Delta\hat{V}$, the charge $\hat{q}_A$ is proportional to $1/\ln(1 + h/r_A)$, where $h = r_B - r_A$ is the current distance between the electrodes. Therefore, reduction of thickness increases the charge in a non-linear manner. On top of this non-linear relation, the current thickness is itself a non-linear function of the applied voltage. The accumulation of charge, in turn, modifies $\Sigma_{\theta r}$, which enters the jump conditions and the governing equation.

Figs. 2(c) and 2(d) display normalized frequencies $\hat{\omega} = \omega H/c_B$, as functions of the normalized wavenumber $\hat{k}$, for thin and thick tubes free of mechanical traction, respectively. It is observed how at infinite wavelength, namely, $\hat{k} = 0$, only the fundamental branches start at the origin. All higher branches initiate at some non-zero cutoff frequencies $\hat{\omega}_c > 0$. The electric actuation shifts $\hat{\omega}_c$ towards higher frequencies. For example, when $\Delta\hat{V} = 2/3$, the cutoff frequency associated with the second mode of the thin tube is about 4 times its initial value when $\Delta\hat{V} = 0$, as it changes from $\sim$3 to $\sim$11.5. A filtering functionality is thus identified with the electric excitation, bearing in mind that only the fundamental mode is propagating at frequencies below $\hat{\omega}_c$. Hence, by subjecting the tube to a bias electric field, we widen a gap at which all non-fundamental modes are filtered. This trend is more pronounced at the thin tube, for which such gaps rendered wider than at the thick tube.

Fig. 3 shows the normalized velocities $\hat{c}$ as functions of the normalized wavenumber $\hat{k}$ for ((a) and (c)) a thin and ((b) and (d)) a thick tube, when axially constrained at ((a) and (b)) $\tilde{\lambda}_z = 1$, and ((c) and (d)) $\tilde{\lambda}_z = 2$. Note that when $\tilde{\lambda}_z = 1$, greater values of $\Delta\hat{V}$ can be applied before the tube collapses, in comparison to the unconstrained setting. Curves associated with $\Delta\hat{V} = 1$ are chosen to be shown instead of $\Delta\hat{V} = 2/3$, and are denoted by the continuous curves with diamond marks (purple). Conversely, tensile axial strain

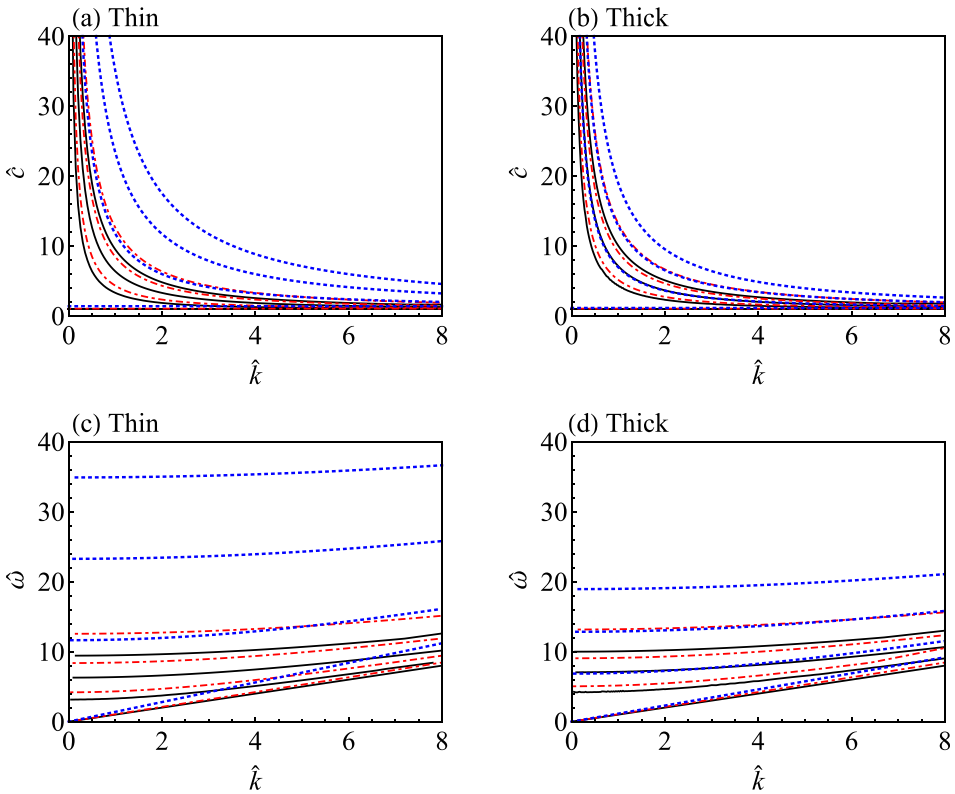

FIG. 2. *Axially free tube*. Normalized ((a) and (b)) velocities $\hat{c}$ and ((c) and (d)) frequencies $\hat{\omega}$ as functions of the normalized wavenumber $\hat{k}$ for ((a) and (c)) a thin and ((b) and (d)) a thick tube. The continuous, dotted-dashed (red), and dotted (blue) curves correspond to the normalized voltages $\Delta\hat{V} = 0$, $\frac{1}{2}$, and $\frac{2}{3}$, respectively.

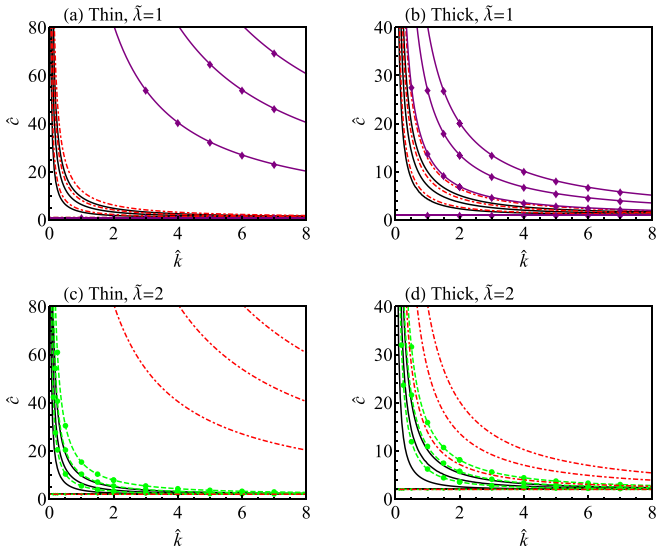

FIG. 3. *Mechanically constrained tube*. Normalized velocities $\hat{c}$ as functions of the normalized wavenumber $\hat{k}$ for ((a) and (c)) a thin and ((b) and (d)) a thick tube, axially constrained at ((a) and (b)) $\tilde{\lambda}_z = 1$, and ((c) and (d)) $\tilde{\lambda}_z = 2$. The continuous curves, dashed curves with bullet marks (green), dotted-dashed curves (red), and continuous curves with diamond marks (purple) correspond to the normalized voltages $\Delta\hat{V} = 0, \frac{1}{3}, \frac{1}{2}$, and 1, respectively.

limits the amount of voltage applied. In particular, at $\tilde{\lambda}_z = 2$, there is no static solution to a loading of $\Delta\hat{V} = 2/3$. Accordingly, there are no corresponding curves. In this case, the figures are supplemented with the dispersion curves at $\Delta\hat{V} = 1/3$, and are denoted by continuous curves with bullet marks (green).

The main observation is the huge velocity enhancement by applying voltage, if the axial strain is fixed. By way of example, examine the velocity of the second mode of the thin tube at $\tilde{\lambda}_z = 1$, $\hat{k} = 2$. Remarkably, when $\Delta\hat{V} = 1$, it is approximately 40 times the velocity when $\Delta\hat{V} = 0$. Again, the cause is not only the resultant strains or geometry; the velocity is about 8 times its counterpart in an elastic tube having the same geometry, and about 15 times its counterpart in an elastic tube with the same geometry and strains.

Similar ratios of enhancement are obtained for the velocity of the second mode of the thin tube at $\tilde{\lambda}_z = 2$, $\hat{k} = 2$, when $\Delta\hat{V} = 1/2$. In this sense, pre-stretching enhances the performance of the tube, meaning that the same result is achieved using less voltage. This is consistent with previous reports on the improvement of dielectric elastomers performance by pre-stretch.[7,38]

These ratios moderate at the thick tube as examination of Figs. 3(b) and 3(d) demonstrate. The velocity of the second mode at $\tilde{\lambda}_z = 1$, $\hat{k} = 2$, $\Delta\hat{V} = 1$, as an example, is about 3 times the velocity when $\Delta\hat{V} = 0$. This moderation at the thick tube in agreement with a similar observation made when axially free tubes were analyzed. It also agrees with the influence of pre-stretch: all point that reduction in thickness promotes velocity enhancement by voltage.

Figs. 4(a) and 4(b) display the normalized frequencies $\hat{\omega}$ as functions of the normalized wavenumber $\hat{k}$ for (a) a thin and (b) a thick tube, axially constrained at $\tilde{\lambda}_z = 1$. The same trends that were observed for unconstrained tubes are

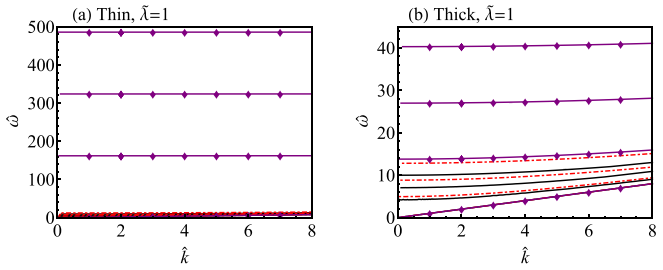

FIG. 4. *Mechanically constrained tube*. Normalized frequencies $\hat{\omega}$ as functions of the normalized wavenumber $\hat{k}$ for (a) a thin and (b) a thick tube, axially constrained at $\tilde{\lambda}_z = 1$. The continuous curves, dot-dashed curves (red), and continuous curves with diamond marks (purple) correspond to the normalized voltages $\Delta\hat{V} = 0, \frac{1}{2}$, and 1, respectively.

identified here. The difference is the significant jump in the frequencies of the modes which undergo drastic velocity rise. For instance, the cutoff frequency of second mode of the thin tube rises from ~3.2 when $\Delta\hat{V} = 0$, to ~163 when $\Delta\hat{V} = 1$. In turn, it implies that bands at which non-fundamental modes attenuate become substantially wider.

To elucidate the steep non-linear change of the dispersion curves as functions of $\Delta\hat{V}$, I turn attention again to Eq. (26), and evaluate $\hat{q}_A/\Delta\hat{V}$ as function of $\Delta\hat{V}$. The relation is plotted in Fig. 5(a) for a thin tube, when clamped at $\tilde{\lambda}_z = 2/3$, 1, and 2, and when it is axially free, denoted by the dashed (orange), dotted (black), dotted-dashed (magenta), and continuous curves, respectively. It is observed how the non-linear finite deformation manifests itself in a drastic rise of charge beyond a certain voltage. The dynamic consequence is the previously mentioned substantial rise in velocity. Fig. 5(a) also explains the relatively limited velocity rise when the tube is not clamped: it collapses before sufficient charge accumulates. In this case, the curve terminates at $\Delta\hat{V} \simeq 0.68$ and $\hat{q}_A/\Delta\hat{V} \simeq 2$, indicated in the figure with the X mark. Conversely, by applying boundary constraints the tube resistance to breakdown increases and the loading path extends, in agreement with related works.[21,23] Therefore, the loading path includes configurations consisting of a sufficient charge to trigger the velocity jump. Further, a comparison of the curves associated with different axial constraints explains why when tensile strain was applied less voltage was needed, as a lower value was sufficient to reach the steep segment of the curve.

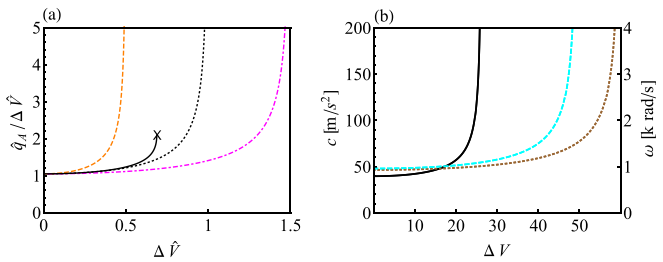

FIG. 5. (a) The ratio $\frac{\hat{q}_A}{\Delta\hat{V}} = \frac{R_A}{H}\ln\frac{\sqrt{AR_B^2+B}}{\sqrt{AR_A^2+B}}$ as function of $\Delta\hat{V}$. The dashed (orange), dotted (black), dotted-dashed (magenta), and the continuous curve correspond to a thin tube when clamped at $\tilde{\lambda}_z = \frac{2}{3}$, 1 and 2, and when it is free to expand, respectively. The X mark denotes the collapse of the tube. (b) The velocities and frequencies of the second mode at wavelength 0.1π mm, as functions of the voltage. The continuous, dashed (cyan), and dotted (brown) curves correspond to the properties of the products Fluorosilicone 730, VHB-4910, and ELASTOSIL RT-625, respectively.

TABLE I. Mass densities, shear moduli, and relative dielectric constants of VHB-4910, ELASTOSIL RT-625, and fluorosilicone 730.

Material	ρ (kg/m^3)	μ (kg/m^3)	ϵ_r
VHB-4910	960	406	4.7
ELASTOSIL RT-625	1020	342	2.7
Fluorosilicone 730	1400	167	6.9

Fig. 5(b) shows the velocities and frequencies of the second mode as functions of the voltage, at a representative wavenumber of $\hat{k} = 2$. To provide a sense for the practical values of the quantities, it is given in a dimensional form, using the properties of three commercially available materials. Hence, the continuous, dashed (cyan), and dotted (brown) curves correspond, respectively, to the products VHB-4910, ELASTOSIL RT-625, and Fluorosilicone 730; Table I provides their approximate physical properties, as found in the literature.[39,40] Similar to the trends exhibited in Fig. 5(a), the curves demonstrate non-linear dependency on the voltage. In particular, these show how a wide range of frequencies and velocities pertains to a relatively small range of applied voltage, which depends on the permittivity-stiffness ratio of the material.

VI. SUMMARY

The equations describing torsional motions of finitely deformed dielectrics were formulated, and were found essentially different from their elastic counterparts. An analytical investigation reveals that the non-dispersive fundamental mode always exists. It also shows how all higher modes converge to that mode in the limit of short waves. To generally determine these modes, a numerical scheme was applied. The resultant dispersion relations were evaluated for different tube thicknesses, axial constraints, and bias electric fields. It was observed how the axial clamping enhances the resistance to breakdown. This, in turn, enabled the primary observation: a drastic rise of the velocities and frequencies of higher modes beyond a certain amount of voltage. The exhibited non-linear dependency indicates that significant changes in these quantities can be induced by relatively small changes in the voltage. The axial constraint promotes the accumulation of sufficient charge to commence this phenomenon. The thickness of the tube affects the amount of voltage needed, as thinner tubes require less voltage.

These results suggest the use of dielectric elastomer tubes as possible mechanisms to accelerate torsional modes across certain frequencies, and their filtering across other frequencies, by tuning the applied voltage.

APPENDIX: THE COMPONENTS OF THE INSTANTANEOUS TENSORS

The non-vanishing components of $\mathcal{A}$, $\mathcal{B}$, and $\mathcal{C}$ on the principal axes of the deformation (17) are

$$\mathcal{A}_{11} = \mathcal{A}_{22} = \mathcal{A}_{33} = \frac{1}{\epsilon}, \tag{A1}$$

$$\mathcal{B}_{121} = \mathcal{B}_{211} = \mathcal{B}_{323} = \mathcal{B}_{233} = \frac{1}{2}\mathcal{B}_{222} = \frac{1}{\epsilon} d_r, \tag{A2}$$

$$\mathcal{C}_{1111} = \mathcal{C}_{2121} = \mathcal{C}_{3131} = \mu\lambda_z^2, \tag{A3}$$

$$\mathcal{C}_{1212} = \mathcal{C}_{2222} = \mathcal{C}_{3232} = \mu\lambda_r^2 + \frac{1}{\epsilon} d_r^2, \tag{A4}$$

$$\mathcal{C}_{1313} = \mathcal{C}_{2323} = \mathcal{C}_{3333} = \mu\lambda_\theta^2, \tag{A5}$$

where the indices $(1, 2, 3)$ correspond to (z, r, θ). The tensors $\mathcal{B}$ and $\mathcal{C}$ are non-homogeneous, since d_r, λ_r, and λ_θ are functions of r.

[1] R. Shankar, T. K. Ghosh, and R. J. Spontak, Soft Matter **3**, 1116–1129 (2007).
[2] A. O'Halloran, F. O'Malley, and P. McHugh, J. Appl. Phys. **104**, 071101 (2008).
[3] P. Brochu and Q. Pei, Macromol. Rapid Commun. **31**, 10–36 (2010).
[4] C. Keplinger, T. Li, R. Baumgartner, Z. Suo, and S. Bauer, Soft Matter **8**, 285–288 (2012).
[5] R. E. Pelrine, R. D. Kornbluh, and J. P. Joseph, Sens. Actuators, A **64**, 77–85 (1998).
[6] R. Pelrine, R. Kornbluh, J. Joseph, R. Heydt, Q.-B. Pei, and S. Chiba, Mater. Sci. Eng., C **11**, 89–100 (2000).
[7] R. Pelrine, R. Kornbluh, Q.-B. Pei, and J. Joseph, Science **287**, 836–839 (2000).
[8] F. Carpi, D. De Rossi, R. Kornbluh, R. Pelrine, and P. Sommer-Larsen, *Dielectric Elastomers as Electromechanical Transducers* (Elsevier, Amsterdam, 2008).
[9] B. Tavakol, M. Bozlar, C. Punckt, G. Froehlicher, H. A. Stone, I. A. Aksay, and D. P. Holmes, Soft Matter **10**, 4789–4794 (2014).
[10] J. Zhu, S. Cai, and Z. Suo, Int. J. Solids Struct. **47**, 3254–3262 (2010).
[11] K. Hochradel, S. Rupitsch, A. Sutor, R. Lerch, D. Vu, and P. Steinmann, Appl. Phys. A **107**, 531–538 (2012).
[12] T. Li, S. Qu, and W. Yang, Int. J. Solids Struct. **49**, 3754–3761 (2012).
[13] G. Shmuel, M. Gei, and G. deBotton, Int. J. Non-Linear. Mech. **47**, 307–316 (2012).
[14] C. Feng, L. Yu, and W. Zhang, Int. J. Non-Linear Mech. **65**, 63–68 (2014).
[15] M. Gei, S. Roccabianca, and M. Bacca, IEEE-ASME Trans. Mechatronics **16**, 102–107 (2011).
[16] G. Shmuel and G. deBotton, J. Mech. Phys. Solids **60**, 1970–1981 (2012).
[17] G. Shmuel, Int. J. Solids Struct. **50**, 680–686 (2013).
[18] J. Zhu, H. Stoyanov, G. Kofod, and Z. Suo, J. Appl. Phys. **108**, 074113 (2010).
[19] L. An, F. Wang, S. Cheng, T. Lu, and T. J. Wang, Smart Mater. Struct. **24**, 035006 (2015).
[20] G. Shmuel and G. deBotton, Proc. R. Soc. A **371**, 20130071 (2013).
[21] B. Li, H. Chen, J. Qiang, S. Hu, Z. Zhu, and Y. Wang, J. Phys. D: Appl. Phys. **44**, 155301 (2011).
[22] T. Lu, J. Huang, C. Jordi, G. Kovacs, R. Huang, D. R. Clarke, and Z. Suo, Soft Matter **8**, 6167–6173 (2012).
[23] J. Zhou, L. Jiang, and R. E. Khayat, Smart Mater. Struct. **23**, 045028 (2014).
[24] B. Li and Z. Zhao, Europhys. Lett. **106**, 67009 (2014).
[25] A. Ozturk and S. Akbarov, Mech. Compos. Mater. **44**, 77–86 (2008).
[26] T. Shearer, I. D. Abrahams, W. J. Parnell, and C. H. Daros, Q. J. Mech. Appl. Math. **66**, 465–487 (2013).
[27] E. Baesu, D. Fortune, and E. Soós, Z. Angew. Math. Phys. **54**, 160–178 (2003).
[28] R. M. McMeeking and C. M. Landis, J. Appl. Mech. **72**, 581–590 (2005).
[29] G. deBotton, L. Tevet-Deree, and E. A. Socolsky, Mech. Adv. Mater. Struct. **14**, 13–22 (2007).
[30] Z. Suo, X. Zhao, and W. H. Greene, J. Mech. Phys. Solids **56**, 467–486 (2008).
[31] A. Dorfmann and R. W. Ogden, Acta Mech. **174**, 167–183 (2005).
[32] A. Dorfmann and R. W. Ogden, IMA. J. Appl. Math. **75**, 603–636 (2010).
[33] M. Singh and A. Pipkin, Arch. Ration. Mech. Anal. **21**, 169–210 (1966).
[34] F. Carpi and D. De Rossi, Mater. Sci. Eng., C **24**, 555–562 (2004).
[35] D. C. Gazis, J. Acoust. Soc. Am. **31**, 568–573 (1959).
[36] D. M. Haughton and R. W. Ogden, J. Mech. Phys. Solids **27**, 489–512 (1979).

[37]S. Roccabianca, M. Gei, and D. Bigoni, IMA J. Appl. Math. **75**, 525–548 (2010).
[38]G. Kofod, J. Phys. D: Appl. Phys. **41**, 215405 (2008).
[39]G. Kofod and P. Sommer-Larsen, Sens. Actuators, A **122**, 273–283 (2005).
[40]R. Kornbluh and R. Pelrine, "High-performance acrylic and silicone elastomers," in *Dielectric Elastomers as Electromechanical Transducers*, edited by F. Carpi, D. D. Rossi, R. Kornbluh, R. Pelrine, and P. Sommer-Larsen (Elsevier, Oxford, UK, 2008), Chap. 4, pp. 33–42.